Supplemental Material for "Superconducting triangular islands as a platform for manipulating Majorana zero modes"

Aidan Winblad[1] and Hua Chen[1,2]

[1] *Department of Physics, Colorado State University, Fort Collins, CO 80523, USA*
[2] *School of Advanced Materials Discovery, Colorado State University, Fort Collins, CO 80523, USA*

I. MANY-BODY BERRY PHASE CALCULATION FOR THE 3-SITE KITAEV TRIANGLE

In this section we provide details for calculating the many-body Berry phase for braiding two MZM in the Kitaev triangle, as shown in Fig. 2 in the main text. To start we use the Hamiltonian Eq. (1) in the main text,

$$\mathcal{H} = \sum_{\langle jl \rangle} (-te^{i\phi_{jl}} c_j^\dagger c_l + \Delta e^{i\theta_{jl}} c_j c_l + \text{h.c.}) - \sum_j \mu c_j^\dagger c_j, \tag{1}$$

and write the creation and annihilation operators in the following Fock space basis for three spinless fermions

$$\begin{aligned}(|0\rangle, |1\rangle, \ldots, |7\rangle) \equiv \{|n_1, n_2, n_3\rangle\} \\ = \big(&|0,0,0\rangle, \\ &|1,0,0\rangle, |0,1,0\rangle, |0,0,1\rangle, \\ &|0,1,1\rangle, |1,0,1\rangle, |1,1,0\rangle, \\ &|1,1,1\rangle\big)\end{aligned}$$

The creation(annihilation) operators in this space are defined as

$$\begin{aligned} c_j^\dagger |n_1, \ldots, n_j, \ldots\rangle &= \sqrt{n_j + 1}(-1)^{s_j} |n_1, \ldots, n_j + 1, \ldots\rangle, \\ c_j |n_1, \ldots, n_j, \ldots\rangle &= \sqrt{n_j}(-1)^{s_j} |n_1, \ldots, n_j - 1, \ldots\rangle, \end{aligned} \tag{2}$$

where

$$s_j = \begin{cases} \sum_{l=1}^{j-1} n_l & j > 1 \\ 0 & j = 1 \end{cases} \tag{3}$$

For the initial configuration corresponding to $\boldsymbol{\phi}_1$ in Eq. (6) of the main text, diagonalizing the 8×8 BdG Hamiltonian in the above basis leads to two degenerate ground states that can be distinguished by the occupation number of the following fermion operator constructed from the two MZM at the two bottom vertices

$$c_M \equiv \frac{1}{2}(a_1 + ib_2),\ n_M \equiv c_M^\dagger c_M \tag{4}$$

The two degenerate ground states for the initial configuration, denoted as $|0\rangle_i$ and $|1\rangle_i$, therefore satisfy

$$\begin{aligned} n_M |0\rangle_i &= 0, \\ n_M |1\rangle_i &= |1\rangle_i \end{aligned} \tag{5}$$

In practice, we first construct the operator R_{gs} as a 8×2 matrix by combining the two column eigenvectors of the two lowest-energy eigenstates of the initial BdG Hamiltonian:

$$R_{\text{gs}} \equiv (\psi_i, \psi_i') \tag{6}$$

and then diagonalize the projected n_M operator:

$$U_n^\dagger (R_{\text{gs}}^\dagger n_M R_{\text{gs}}) U_n \equiv R_i^\dagger n_M R_i = \begin{pmatrix} 0 & \\ & 1 \end{pmatrix} \tag{7}$$

To carry out the Berry phase calculation we next need to adiabatically "rotate" the vector potential field by following the linearly interpolated closed parameter path described in the main text, which is discretized into $N+1$ segments. At any given point labeled by j along the path, we diagonalize the corresponding Hamiltonian and construct the projection operator P_j using the two lowest-energy eigenvectors ψ_j, ψ'_j:

$$P_j \equiv \psi_j \otimes \psi_j^\dagger + \psi'_j \otimes \psi_j'^\dagger \tag{8}$$

where $\otimes$ means tensor product. The 2×2 Berry phase matrix $M_{f\leftarrow i}$ for the given parameter path is then obtained as

$$M_{f\leftarrow i} = \lim_{N\to\infty} R_f^\dagger P_N P_{N-1} \dots P_1 R_i \tag{9}$$

where $R_f = R_i$ since the path is closed.

By using a large enough N we found the converged $M_{f\leftarrow i}$ matrix has only diagonal elements being nonzero, meaning the braiding only changes each ground state by a scalar phase factor. Their values are $(M_{f\leftarrow i})_{00} = e^{i0.118\pi}$ and $(M_{f\leftarrow i})_{11} = e^{-i0.382\pi} = e^{i(0.118-0.5)\pi}$.

We end this section by noting that the parameter path considered for the 3-site Kitaev triangle above is not equivalent to rotating a staggered vector potential but to separately manipulating the Peierls phases along the three edges. We have also done calculations for the latter case and found the two lowest-energy states fail to be degenerate everywhere along the parameter path, leading to non-standard relative Berry phases between the two initial states.

II. CORNER MZM IN FINITE-WIDTH HOLLOW TRIANGLES

A model that is closer to a realistic hollow triangular island is the finite-width triangular chain or ribbon. An example, illustrated in Figure 1 (c), has its edge length $L = 50$ and width $W = 3$. The phase diagram Fig. 1 (a) is created in a similar way as that in Fig. 3 (a) of the main text, assuming a constant vector potential and infinitely long $W = 3$ ribbons. The spectral flow for the actual triangle with $\mu = 1.6$ in Fig. 1 (b) shows MZM in the parameter regions in agreement with the phase diagram. Fig. 1 (c) plots the MZM wavefunction for $A = 2.7409$ and $\mu = 1.6$ that are indeed well localized at the bottom corners.

We next rotate the uniform vector potential to examine how the MZM move on a hollow triangle. Figure 2 shows the spectral flow and eigenfunctions as we rotate $\varphi = 0$ to $\varphi = \pi$ counterclockwisely. The two MZM cycle through the three vertices in a similar manner as that in Fig. 4 of the main text (only the MZM wavefunctions at $\varphi = 0$ and $\frac{\pi}{3}$ are plotted as representatives of the $\varphi = n\pi/3$ cases). Note that the spectral flow has 3-fold rotation symmetry but not 6-fold, since increasing φ by $\frac{2\pi}{3}$ is equivalent to rotating the coordinate system clockwisely by $\frac{2\pi}{3}$. In contrast, rotating the vector potential by $\frac{\pi}{3}$, if without an additional sign change of the p-wave pairing potential, is not an exact symmetry of the finite triangle. Also we did not try to scrutinize the phase diagram to find a parameter path in which the bulk gap does not close, as in the $W = 1$ case in the main text. Here we just point out that identifying a system-specific parameter path for adiabatic manipulation of MZM is in principle always possible, especially if one is allowed to have more knobs other than φ in real structures, such as tuning the chemical potential of individual edges or the size of the vector potential, etc.

III. BRAIDING MZM IN A SMALL NETWORK OF TRIANGLES

In this section we show that one can braid two out of four MZM, a minimal setting for nontrivial manipulation of the degenerate many-body ground states, by using a small network of corner-sharing triangles. We focus on the critical step of swapping γ_2 and γ_3 as labeled in Fig. 5 of the main text. This can be done by rotating the vector potential of the triangle in the middle of the bottom row from $\varphi = \frac{\pi}{6}$ to $\frac{\pi}{3}$. More specifically, when $\varphi = \frac{\pi}{6}$, with the chosen values of μ and A, only the right edge of the said triangle is topologically nontrivial. The chain that hosts $\gamma_{3,4}$ thus extends through this nontrivial edge to the top triangle as in Fig. 3 (b). On the other hand, when φ increases to $\frac{\pi}{3}$, the nontrivial edge of the middle triangle changes from right to left, which leads to γ_2 hopping from its left corner to the right through the top corner, while γ_3 is unaffected [Figs. 3 (c-g)]. As a result the γ_2, γ_3 swapping is done without closing the bulk gap, as can be seen from the spectral flow in Fig. 3 (a).

(a)

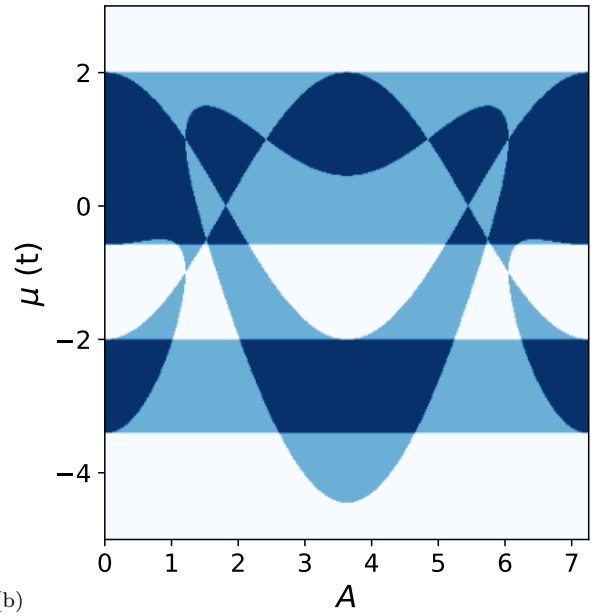

(b)

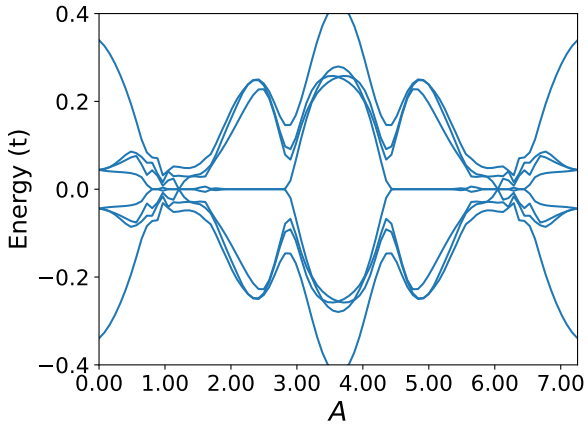

(c)

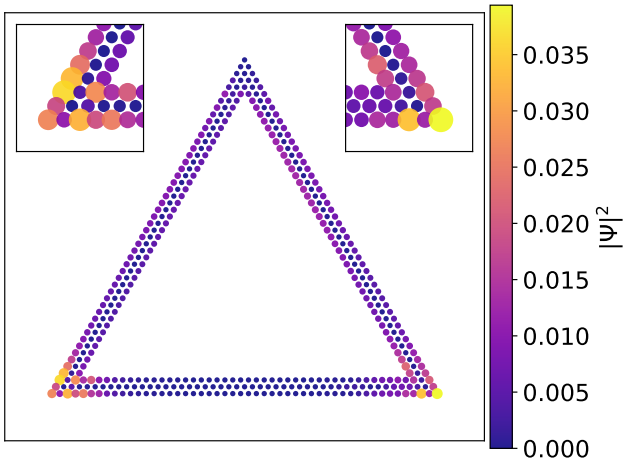

FIG. 1. (a) Topological phase diagram for a $W = 3$ hollow triangle obtained by overlapping the $\mathcal{M}(A, \mu)$ plots of 1D chains with $\mathbf{A} = A\hat{\mathbf{y}}$ and $\mathbf{A} = A(\frac{\sqrt{3}}{2}\hat{\mathbf{x}} + \frac{1}{2}\hat{\mathbf{y}})$. Color scheme: white—$\mathcal{M} = 1$, dark blue—$\mathcal{M} = -1$, light blue—$\mathcal{M} = 0$ (b) Near-gap BdG eigen-energies vs A for a finite triangle with edge length $L = 50$, $W = 3$, and $\mu = 1.6$. (c) BdG eigenfunction $|\Psi|^2$ summed over the two zero modes at $A = 2.4709$.

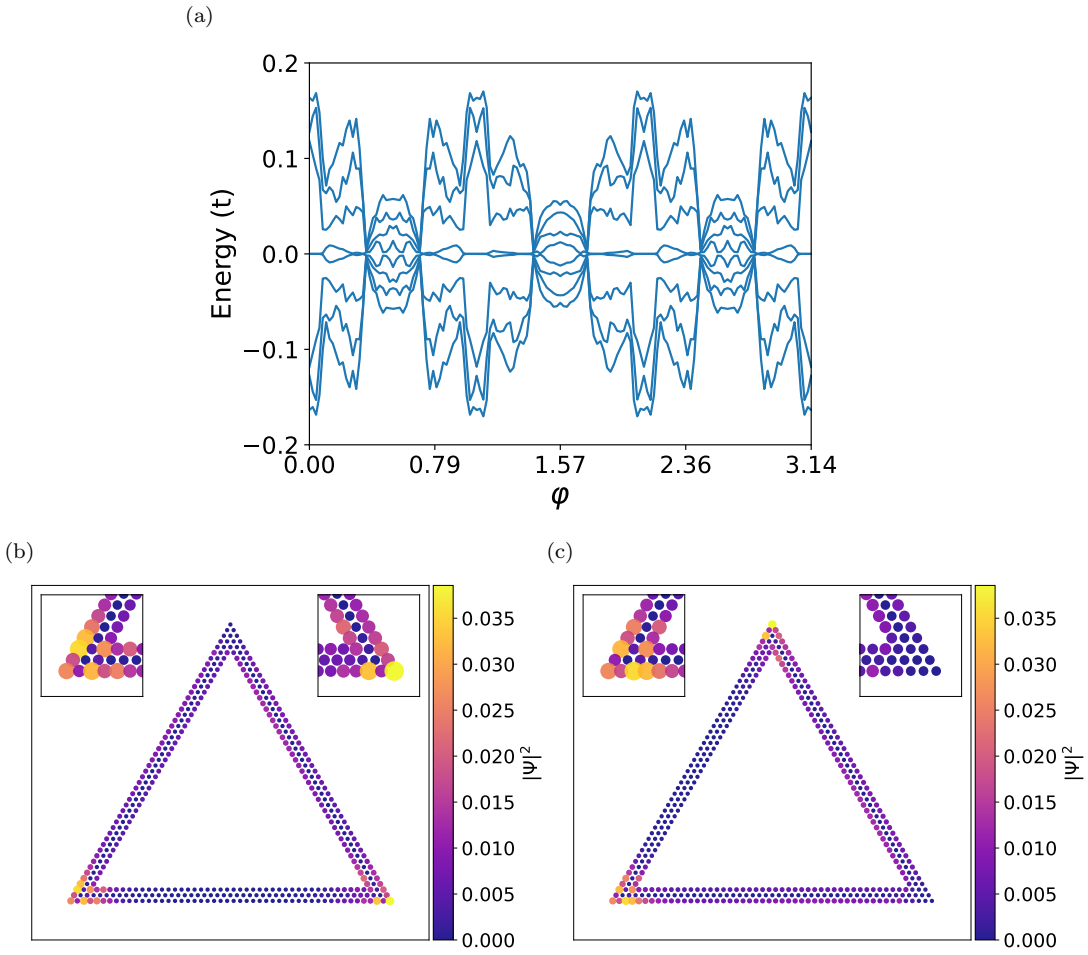

FIG. 2. (a) Spectral flow of a hollow triangle with $W = 3$, $L = 50$, $\mu = 1.6$, and $A = 2.75$ with increasing rotation angle φ, defined through $\mathbf{A} = A(-\sin\varphi\hat{\mathbf{x}} + \cos\varphi\hat{\mathbf{y}})$. (b-c) BdG eigenfunction $|\Psi|^2$ summed over the two zero modes at $\varphi = 0$ and $\frac{\pi}{3}$, respectively.

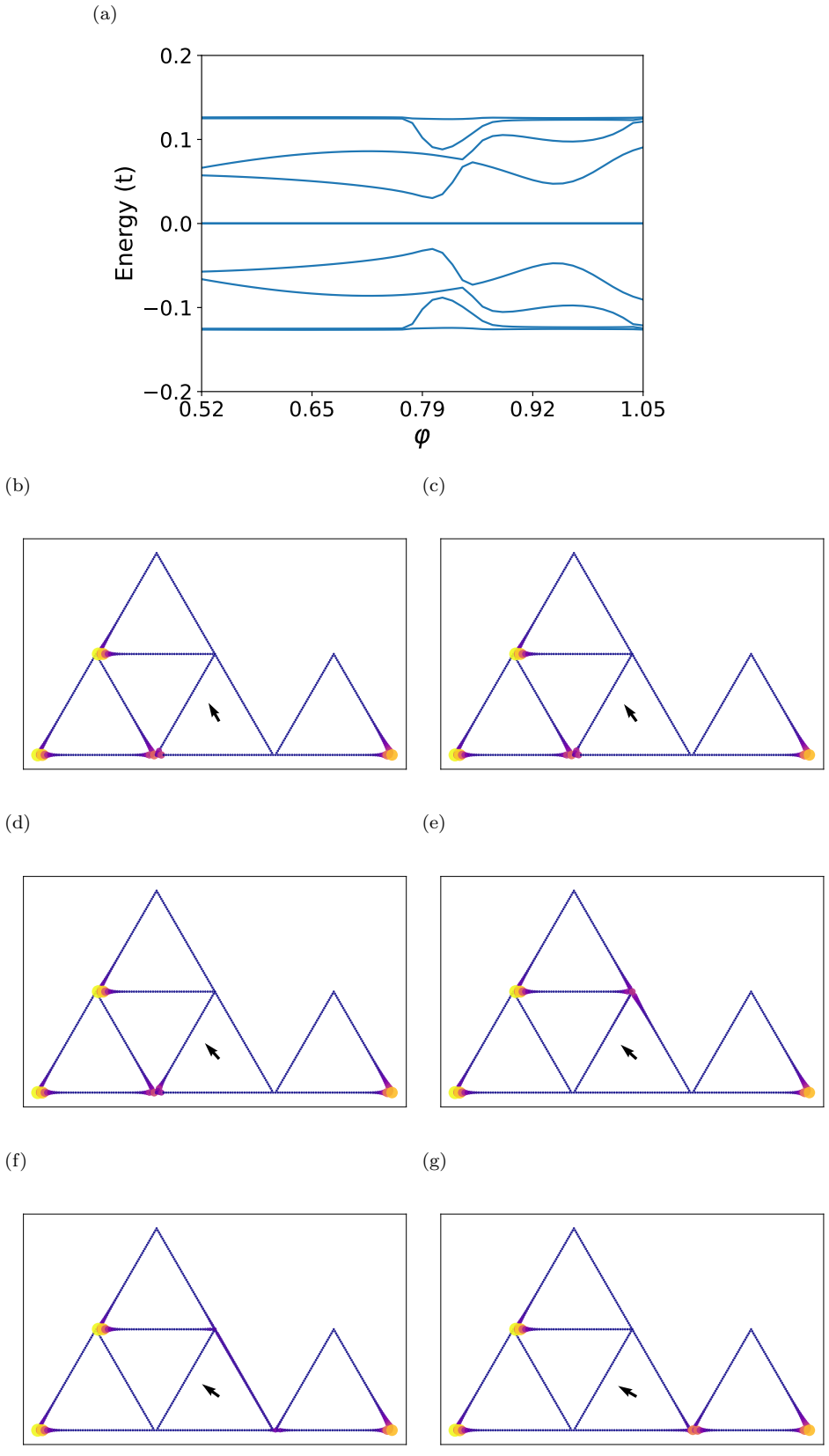

FIG. 3. (a) Spectral flow for the critical step of swapping γ_2 and γ_3 in the example of Fig. 5 in the main text, calculated using four corner-sharing triangles of $W = 1$ and $L = 50$, with $\mu = 1.6$ and $A = 2.6$. Vector potential for the middle triangle in the bottom row can rotate according to $\mathbf{A} = A(-\sin\varphi\hat{\mathbf{x}} + \cos\varphi\hat{\mathbf{y}})$ from $\varphi = \frac{\pi}{6}$ to $\frac{\pi}{3}$, while the other three have fixed $\varphi = 0$. (b)-(g) BdG eigenfunction $|\Psi|^2$ summed over the four zero modes at equally-spaced points along the rotation path. The black arrow indicates the direction of the vector potential for the bottom middle triangle.